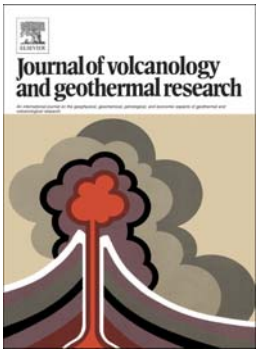

Cap rock efficiency of geothermal systems in fold-and-thrust belts: Evidence from paleo-thermal and structural analyses in Rosario de La Frontera geothermal area (NW Argentina)

R. Maffucci, S. Corrado, L. Aldega, S. Bigi, A. Chiodi, L. Di Paolo, G. Giordano, C. Invernizzi

PII: S0377-0273(16)30403-6
DOI: doi: 10.1016/j.jvolgeores.2016.10.008
Reference: VOLGEO 5944

To appear in: *Journal of Volcanology and Geothermal Research*

Received date: 14 June 2016
Revised date: 11 October 2016
Accepted date: 15 October 2016

Please cite this article as: Maffucci, R., Corrado, S., Aldega, L., Bigi, S., Chiodi, A., Di Paolo, L., Giordano, G., Invernizzi, C., Cap rock efficiency of geothermal systems in fold-and-thrust belts: Evidence from paleo-thermal and structural analyses in Rosario de La Frontera geothermal area (NW Argentina), *Journal of Volcanology and Geothermal Research* (2016), doi: 10.1016/j.jvolgeores.2016.10.008

Cap rock efficiency of geothermal systems in fold-and-thrust belts: evidence from paleo-thermal and structural analyses in Rosario de La Frontera geothermal area (NW Argentina)

R. Maffucci[1,2], S. Corrado[1], L. Aldega[3], S. Bigi[3], A. Chiodi[4], L. Di Paolo[5], G. Giordano[1], C. Invernizzi[6]

[1] Dipartimento di Scienze, Università Roma Tre, L.go San Leonardo Murialdo 1, 00146 Roma, Italy
corresponding author: sveva.corrado@uniroma3.it
[2] Dipartimento di Scienze Umanistiche, della Comunicazione e del Turismo, Università degli Studi della Tuscia, Via S. Maria in Gradi, 4, 01100 Viterbo, Italy
[3] Dipartimento di Scienze della Terra, Sapienza Università di Roma, P.le Aldo Moro 5, 00185 Roma, Italy
[4] GEONORTE-INENCO (UNSa-CONICET), Av. Bolivia 5150, A4400FVY Salta, Argentina
[5] Eni E&P Division, San Donato Milanese, 20097 Milano, Italy
[6] Scuola di Scienze e Tecnologie, Università di Camerino, Via Gentile III da Varano, 62032 Camerino, Italy

Abstract

Cap rock characterization of geothermal systems is often neglected despite fracturing may reduce its **efficiency** and favours fluid migration. We investigated the siliciclastic cap rock of Rosario de La Frontera geothermal system (NW Argentina) in order to assess its quality as a function of fracture patterns and related thermal alteration.

Paleothermal investigations (XRD on fine-grained fraction of sediments, organic matter optical analysis and fluid inclusions on veins) **and** 1D thermal modelling **allowed us** to distinguish the thermal fingerprint associated to sedimentary burial from that related to fluid migration.

The geothermal system is hosted in a Neogene N-S anticline dissected by high angle NNW- and ENE-**striking** faults. Its cap rock can be grouped into two quality categories:

- **rocks acting as good insulators, deformed by NNW–SSE and E–W shear fractures, NNE-SSW gypsum- and N-S-striking calcite-filled veins that developed during the initial stage of anticline growth. Maximum paleo-temperatures (<60 °C) were experienced during deposition to folding phases.**
- **rocks acting as bad insulators, deformed by NNW-SSE fault planes and NNW- and WNW-striking sets of fractures associated to late transpressive kinematics.** Maximum paleo-temperatures higher than about 115 °C are linked to fluid migration from the reservoir to surface (with a reservoir top at maximum depths of 2.5 km) along fault damage zones.

This multi-method approach **turned out** to be particularly useful to trace the main pathways of hot fluids and can be applied in blind geothermal systems where either subsurface data are scarce or surface thermal anomalies are lacking.

Keywords:
Geothermal systems
Cap-rock
Mixed layers illite-smectite
Vitrinite reflectance
Fluid inclusions
Santa Bárbara system
NW Argentina

1. Introduction

Characterization of geothermal systems is strongly focu**s**sed on **quality** assessment of reservoir rocks by evaluating and predicting primary and secondary permeability (Dobson et al., 2013; Giordano et al., 2013; Invernizzi et al., 2014). As most geothermal reservoirs are hosted in fractured rock media, scientific studies deal with analyses and modelling of fracture network (Barton et al., 1997; Wang and Ghassemi, 2011; Ghassemi, 2012; Müller et al., 2010; Maffucci et al., 2012, 2013, 2015; Rahman and Rahman 2013; Phillip, 2015).

Less attention has been generally addressed to the characterization of cap rock**s** of geothermal systems that may dominantly contribute to the maintenance of enthalpy **and temperature** through time (Todesco and Giordano, 2010). Cap-rock **efficiency** , is mainly evaluated by thickness (Timlin, 2009), thermal alteration (Corrado et al., 2014) and integrity determinations (Carapezza et al., 2015) but can be affected and reduced by fracturing related to folding, thrusting and tectonic inversion. In turn, fracture patterns may trigger hot fluid circulation and neoformation of temperature-dependent minerals that may provide insights on levels of thermal alteration (Rossetti et al, 2011; Corrado et al. 2014; Vignaroli et al., **2015**).

In this paper, we discuss the relationship between fracturing and thermal alteration of the cap rock **of** the Rosario de La Frontera geothermal system in the outer zone of the Andean retrowedge (NW Argentina). This active geothermal system is characterized by several hot springs mainly occurring at the northern edge of the Sierra de La Candelaria anticline, close to the town of Rosario de La Frontera (Moreno Espelta et al., 1975;

Seggiaro et al., 1995; Pesce and Miranda, 2003; Invernizzi et al., 2014; Chiodi et al., 2015). At depths, reservoir rocks are fractured sandstones of the Cretaceous syn-rift deposits (Pirgua Subgroup) and cap rocks are **low permeability** post-rift and syn-orogenic deposits (Balbuena and Santa Bárbara Subgroups, and Metán Subgroup respectively; Moreno Espelta et al., 1975; Seggiaro et al., 1995, 2015; Invernizzi et al., 2014; Chiodi et al., 2015; Maffucci et al., 2015).

X-ray diffraction of clay minerals, organic matter optical microscopy and fluid inclusions microthermometry and petrography on veins fillings (Aldega et al., 2007; Corrado et al., 2010) allowed unraveling the thermal evolution of the couple reservoir + cap rock of the geothermal system with the aid of 1D conductive thermal modelling. The comparison among features and distribution of fractures and paleothermal indicators allowed **us to define** the main pathways of hot fluids and their role onto thermal alteration of the cap rock by distinguishing the thermal fingerprint associated to sedimentary burial from that related to fluid migration.

The tectonic evolution of the Sierra de La Candelaria ridge during the Andean orogeny is a common example of positive inversion producing deformation patterns at various scales. The identification of modes and sequence of deformation, as well as of the paleothermal imprint of the fracture patterns, opens new perspectives on the detection of cap rock efficiency of geothermal systems hosted in fold-and-thrust belts. This approach, traditionally used in oil and gas exploration, represents a straightforward and brand-new workflow to be applied in areas of complex deformation patterns.

2. Geological setting

In NW Argentina, the most external and less culminated structures of the Andean retro-wedge crop out in the Subandean foreland fold-and-thrust belt (Fig. 1). These structures generally consist of anticlines mainly associated with thrusts or reverse faults formed during the Cenozoic Andean shortening (Allmendiger et al., 1983; Jordan et al., 1983; Jordan and Allmendiger, 1986; Salfity et al., 1993; Cristallini et al., 1997; Reynolds et al., 2000; Iaffa et al., 2013). However, along-strike differences in tectonic style led to subdivide the Subandean foreland fold-and-thrust belt into three different structural provinces that are, from north to south, the thin-skinned Subandean Ranges, the thick-skinned Santa Bárbara System and the deep-seated basement thrust of the Sierra Pampeanas (Ramos, 1999; Kley et al., 1999; Kley and Monaldi, 2002; Fig. 1).

In NW Argentina (NOA), numerous thermal springs, associated to medium- and low-enthalpy geothermal systems, occur along the positive structures of these different foreland segments (Pesce and Miranda, 2003). Among them, Rosario de La Frontera, in the Salta province, represents one of the most important geothermal systems for the high temperature of its hot springs (up to about 90 °C at surface; Seggiaro et al., 1995, 2015; Pesce and Miranda, 2003; Chiodi et al. 2012a, 2012b, 2015; Invernizzi et al., 2014). This geothermal system belongs to the Sierra de La Candelaria anticline cropping out in the southernmost portion of the Santa Bárbara System (Kley et al., 1999; González et al. 2000; Salfity and Monaldi 2006; Fig. 1). Sierra de La Candelaria consists of an about 50 km-long and up to ten km-wide asymmetrical anticline developed at the hanging wall of a N-S high-angle inverted normal fault bordering the anticline to the east (Iaffa et al., 2013; Seggiaro et al., 1997, 2015; Maffucci et al., 2015; Fig. 2a). The main stratigraphic units and the related tectonic events that characterized the anticline are summarised in the chronostratigraphic scheme of figure 2b. The Precambrian basement (Medina Formation) made up of low grade metasedimentary rocks crops out at the anticline core (**Bossi, 1969; Ramos, 2008;** Figs. 2a, b). The oldest rocks that unconformably overlie the basement belong to the Cretaceous to Paleogene continental rift deposits of the Salta Group comprising three units that are, from bottom to top: Pirgua, Balbuena and Santa Bárbara Subgroups (Moreno, 1970; Reyes and Salfity, 1973; Salfity and Marquillas, 1981; Gómez Omil et al., 1989). The Pirgua Subgroup is interpreted as a syn-rift deposit associated to the formation of the Salta Basin, whose deposition was strongly controlled by extensional faults (Turner, 1959; Fig. 2b). The Pirgua Subgroup is mainly represented by red breccias, conglomerates, sandstones and shales of continental origin, deposited in alluvial fans and fluvial plains environments (Gómez Omil et al., 1989; Moreno, 1970; Reyes and Salfity, 1973; Salfity and Marquillas, 1981). To the top, these deposits evolve into the post-rift Balbuena and Santa Bárbara Subgroups (Salfity and Marquillas, 1981; Turner, 1959; Fig. 2b). These Subgroups are mainly represented by limestones **of the Yacoraite Fm**and shales **of the Mealla Fm** deposited in lacustrine, shallow marine **and continental environments** (Moreno, 1970; Bonaparte et al., 1977; Marquillas et al., 2005).

The Orán Group (Middle Miocene-Pleistocene, Russo and Serraiotto, 1979) widely crops out in the northern **sector** of the anticline**,** unconformably overlying the Salta Group. The Orán Group includes the lower Metán and the upper Jujuy Subgroups (Figs. 2a, b). In the study area, the Metán Subgroup is mainly constituted by the Anta Fm that has a thickness

up to about 700 m (Moreno Espelta et al., 1975) and is made up of well stratified sandstone**s**, laminated shale**s** and massive quartzarenite**s with** gypsum **interlayers**. The Anta Fm is overlied by the sandstone-dominated Jesús María Fm (Metán Subgroup) with a thickness of about 450 m and the gravel-rich sandstones of the Guanaco Fm (Jujuy Subgroup), about 500 m thick (Moreno Espelta et al., 1975).

The kinematic evolution of the Sierra de La Candelaria anticline was recently described by Maffucci et al. (2015) who consider a multi-stage evolutionary model characterized by positive inversion of a rift related-normal fault, strike-slip and extensional tectonics. Accordingly, the anticline formed as the result of the reactivation, during the Andean orogenesis, of a N-S Cretaceous normal fault bordering the anticline along its eastern margin (Iaffa et al., 2011). The **subsequent** development of **a NNW-SSE-striking** transpressive fault with a left-lateral strike-slip component, led to a positive flower-like structure. Furthermore, E-W normal faults, dissecting the anticline in its central portion, formed in the final stage of folding to accommodate fold culmination (Maffucci et al., 2015).

The conceptual model of fluid circulation consists of two aquifers developed at different depths and detected on the basis of geochemical, hydrogeological (Invernizzi et al., 2014; Chiodi et al., 2015) and audio-magnetotelluric (Barcelona et al., 2013) investigations. The deepest hydrothermal reservoir, hosted within the Cretaceous Pirgua Subgroup deposits, is mainly recharged by meteoric water (Invernizzi et al., 2014; Chiodi et al., 2015; Seggiaro et al., 2015) and shows a Na–HCO_3 composition with significant contributions of crustal CO_2 and He from mantle degassing (Chiodi et al., 2015). The uprising thermal fluids mix with a relatively high salinity Na–Cl dominated shallower aquifer produced by the interaction of meteoric water with **evaporite** deposits of the Anta Fm (Chiodi et al., 2015).

As a result, in proximity of the northern plunge of the ridge, close to the Hotel Termas spa and a few km to the south of Rosario de La Frontera village, several hot springs occur (Fig. 2a). They record surface temperatures up to 90°C (Pesce and Miranda 2003; Chiodi et al. 2012a, 2012b, 2015; Fig. 3a).

3. Methods and materials

A suite of 23 samples for paleothermal analyses was collected from the Pirgua Subgroup and Yacoraite, Anta and Jesús María Fms along the Sierra de La Candelaria anticline either far away from hot springs, to check the maximum burial conditions of the sedimentary succession (Anta Yaco area), or close to hot springs, to determine hydrothermal fluid alteration (Hotel Termas area) (Fig. 2a). In detail, in the Anta Yaco area,

samples for X-ray diffraction (XRD) analysis come from the thick arenaceous-pelitic beds of the Pirgua Subgroup, and from the **siltite** and **pelite** layers of the Yacoraite and Anta Fms. Close to hot springs, **pelite** layers of the Anta and Jesús María Fms were **sampled** (Figs. 2 and 3; Table 1).

For the organic matter optical microscopy analysis, samples belong to organic-rich layers of the Yacoraite Fm that were collected in the south-western limb of the anticline (Anta Yaco area) (Figs. 2 and 3a; Table 1).

Samples for fluid inclusion studies were collected from calcite and gypsum-filled veins occurring in the Anta Fm, in the Hotel Termas area (Fig. 3a; Table 1).

3.1 X-Ray Diffraction

Qualitative and semi-quantitative analyses of whole-rock composition and of the < 2 μm grain-size fraction (equivalent spherical diameter) were performed with a Scintag X1 X-ray system (CuKα radiation) at 40 kV and 45 mA. Randomly oriented whole-rock powders were run in the 2–70° 2θ interval with a step size of 0.05° 2θ and a counting time of 3 s per step. Oriented air-dried and ethylene-glycol solvated samples were scanned from 1 to 48° 2θ and from 1 to 30° 2θ respectively with a step size of 0.05° 2θ and a count time of 4 s per step. The illite content in mixed layers I–S was determined according to Moore and Reynolds (1997) by using the delta two-theta method after decomposing the composite peaks between 9 and 10° 2θ and 16–17° 2θ. The I–S ordering type (Reichweite parameter, R; Jagodzinski, 1949) was determined by the position of the I001-S001 reflection between 5 and 8.5° 2θ (Moore and Reynolds, 1997). The term R expresses the probability, given a layer A, of finding the next layer to be B. The R parameter may range from 0 to 3. R0 means that there is no preferred sequence in stacking of layers and that illite and smectite layers are stacked randomly along the c-axis; R1 indicates that a smectite layer is followed by an illite layer and that the order of stacking of layers appears in the interstratification sequence; R3 indicates long-range ordering and that each smectite layer is surrounded by at least three illite layers on each side.

3.2 Organic Matter Optical Microscopy Whole-rock samples were mounted in epoxy resin and polished according to standard procedures described in Bustin et al. (1990). Vitrinite reflectance (R_o%) measurements were performed on randomly oriented grains using the MSP200 equipment on a Zeiss Axioplan microscope, under oil immersion in reflected monochromatic non-polarized light. On each sample, measurements were

carried out on unaltered, non-oxidized, and unfractured fragments of vitrinite macerals. Mean reflectance values were calculated from the arithmetic mean of these measurements.

3.3 Fluid Inclusion Analyses

An accurate petrographic analysis was performed on 200 μm-thick, doubly-polished wafers to distinguish among different fluid inclusion assemblages (FIAs). In particular, primary and secondary fluid inclusions, and FIAs related to different growth stages of extension veins were distinguished. Small fragments of these wafers were selected for microthermometric determinations, carried out by an USGS heating-freezing stage calibrated at 0 °C, − 56.6 °C and 374 °C with synthetic standards. Measurement accuracy is about ± 1 °C for heating runs and ± 0.1 °C for freezing runs. Freezing and heating measurements over two-phase liquid/vapour inclusions were repeated twice or three times in order to obtain an average and representative value for (1) ice melting temperature (Tm ice) and (2) total homogenization temperature (Th total) (Diamond, 2003). Fluid inclusions showing anomalous vapour–liquid ratios, necking-down phenomena or deformation due to intense twinning in calcite crystals were discarded. Th total has been used to define the minimum trapping temperature during crystallization when re-equilibration processes were negligible.

3.4 One-dimensional thermal modelling

Burial and thermal history of **the** Cretaceous-Neogene sedimentary succession was **performed** by BASIN MOD-1D (1996) software. Input are from stratigraphic and structural data (e.g., age and thicknesses of sedimentary units and age of depositional/exhumation events **such as** burial, uplift and erosion), physical features of rock units available from software libraries and literature (pure and mixed lithologies, age and thermal conductivity) and regional geothermal gradient values (Seggiaro et al., 1995, 2015; Reynolds et al., 2000; Marquillas et al., 2005; Carrapa et al., 2011; Hain et al., 2011; Invernizzi et al., 2014). The main assumptions for 1D modelling are: (1) rock decompaction factors apply only to clastic deposits according to Sclater and Christie's method (1980); (2) sea level changes are neglected as the thermal evolution is influenced more by sediment thickness than water depth (Butler, 1992); (3) thermal modelling was performed through LLNL Easy %Ro method (Sweeney and Burnham, 1990); (4) different geothermal gradients for the syn-rift (45 °C/km), post-rift and syn-orogenic sedimentation (40 °C/km) guaranteed the

best fit of paleo-thermal data (Seggiaro et al., 1995, 2015; Di Paolo et al., 2012; Invernizzi et al., 2014; Chiodi et al., 2015).

Burial curves were calibrated against R_o% and I% in **mixed layers** I-S , according to the paleothermal correlation proposed by Merriman and Frey (1999) and modified by Caricchi et al. (2015).

4. Results

4.1 Structural analyses

Structural analyses were performed along the Sierra de La Candelaria anticline both far away and close to hot springs (Anta Yaco and Hotel Termas area, respectively) in order to understand the influence of different discontinuities, and of the related deformation events affecting the anticline, on fluids migration. **More than 200 structural data allowed us to recognize the deformation phases that affected the anticline during its evolution.**

In the Anta Yaco area, far away from hot springs, the Pirgua Subgroup and Yacoraite Fm are characterized by E-W-striking syn-folding shear fractures dipping 80° to SE with right-lateral sense of motion (Figs. 4a, b). Shear fractures are organized in a systematic set with a regular spacing of 15 cm in the sandstones of the Pirgua Subgruop, which increase up to 30 cm in the limestones of the Yacoraite Fm. This systematic fracture set is interpreted as the result of the initial stage of folding of the Sierra de La Candelaria ridge due to the WNW-ESE Andean shortening (Marrett et al., 1994; Maffucci et al., 2015). The Anta Formation shows a pervasive system of conjugate and subvertical shear fractures striking NNW–SSE and E–W. They are interpreted as Type I fracture array of Stearns (1968) and are consistent with the Andean shortening direction (Fig. 4c).

Differently, in the Hotel Termas area, close to hot springs, both syn-folding and post-folding features were observed in the Anta Fm. Syn-folding features are mainly represented by bedding parallel gypsum-filled veins that strike NNE-SSW (Figs. 5a, d). Gypsum veins have a rectilinear shape and millimetric thickness. Gypsum within the veins grows either perpendicular or oblique to the vein walls. The former orientation of gypsum crystals indicates layer decompression (σ3 normal to bedding, σ1 horizontal) associated to the initial stage of folding whereas oblique crystals grow as result of shear along bedding (flexural slip).

N-S-striking joints and calcite-filled veins are also interpreted as syn-folding features suggesting an extension sub-parallel to the fold axis trend (Fig. 5d).

Conjugate systems of subvertical shear fractures roughly striking NNW–SSE and E–W occur as well (Type I; Stearns, 1968).

The development of NNW-SSE oblique fault planes and the occurrence of NNW- and WNW-striking sets of fractures and calcite-filled veins are the result of the second phase of deformation that affected the Sierra de La Candelaria ridge linked to transpressive kinematics. Fault segments strike NNW-SSE and steeply dip to SW with a dominant strike-slip motion (slickenlines pitch lower than 25°) and a minor left-lateral kinematics (Figs. 5b, d). Subsidiary Riedel planes strike N50°W with slickenlines striking N330° and N290°.

E–W and ENE-WSW-striking normal fault planes dipping to the north, record the final stage of the anticline development indicating an extension perpendicular to fold axis (Figs. 5c, d). Slickenlines on fault planes often show the superposition of a dip-slip motion (slickenlines pitch between 70° and 120°).

4.2 X-Ray Diffraction

Rocks with syn-folding features

In the anta Yaco area, far away from the hot springs, the top of the Anta Fm is mainly composed of phyllosilicate minerals (68%) and subordinate amounts of plagioclase (23%), quartz (7%) and k-feldspar (2%) (Table 1). In the < 2 μm grain-size fraction, mineralogical assemblage of sample AR11 collected at the top of the **f**ormation differs from that of sample AR29 collected at its base. The top layer is constituted by mixed layers I-S (67%), illite (32%) and **minor** amounts of chlorite (1%) whereas the bottom layer is mainly characterized by an illite-rich composition (85%) followed by chlorite (10%) and mixed layers I-S (5%). Mixed layers I-S are random ordered structures with an illite content of 25% for the top layer and 50% for the base of the Anta Fm (Figs. 3, **6**a).

The underlying Yacoraite Fm is generally characterized by phyllosilicate (73-89%), albite (5-12%) and quartz (3-8%), and small amounts of k-feldspar that do not exceed 2%. Occasionally, zeolite minerals such as laumontite and analcime, carbonate minerals as calcite and iron oxides occur (Table 1). Among the phyllosilicates, illite and mixed layers I-S are the main constituents of the clay fraction whose contents depend on the sampled lithology. In detail, illite prevails on mixed layers I-S in silt-rich layers (AR10), and the reverse is true for clay-rich layers (AR5 and AR7) where the weight percent of mixed layers I-S ranges from 79 to 86% (Table 1). Mixed layers I-S are mainly constituted by random ordered structures (R0) with an illite content of 20% that indicates the diagenetic signal of the basin. Only in sample AR7b two populations of mixed layers I-S coexist,

indicating a detrital supply derived from high thermal maturity rocks (long range ordered structures R3) which superimposes on the diagenetic phases (R0 I-S) (Fig. 3).

In the syn-rift deposits of the Cretaceous Pirgua Subgroup, illite and mixed layers I-S occur in the < 2 μm grain-size fraction with amounts of 80% and 20%, respectively. Two populations of mixed layers I-S have been identified, one is represented by high expandable mixed layers I-S with an illite content of 20%, the other by short range ordered structures (R1) with an illite content of 75% (Table 1, Fig. 3).

Fine-grained sandstones of the Miocene Jesús María Fm, **close to hot springs,** display a whole rock composition made of phyllosilicate minerals (72%), quartz (12%), plagioclase (10%), calcite (4%) and hematite (2%) (Table 1). The clay fraction is composed of 91% of mixed layers I-S and low amounts of illite (7%) and chlorite (2%). Mixed-layers I-S are random ordered structures with illite layers of 20%.

The underlying Anta Fm is generally characterized by phyllosilicates (70-85%), plagioclase (3-6%), quartz (2-16%), analcime (1-7%) and small amounts of k-feldspar (2%). Occasionally, carbonate minerals such as calcite and ankerite, and gypsum occur as veins filling (AR19b) or in the matrix of fractured rocks.

Two lithology dependent mineral assemblages were found in the clay fraction. Shales (AR1, AR16, AR17) are mixed layers I-S rich (>70%), with subordinate amounts of illite and traces of chlorite. Siltites (AR19, AR21) are illite rich with amounts higher than 79% and contain mixed layers I-S. Chlorite occasionally occur**s**.

Mixed-layers I-S for both lithologies are random ordered structures with an illite content ranging between 20 and 30%.

Rocks with post-folding features

A complex association of mixed layered clay minerals was found in the < 2 μm grain-size fraction of the Anta Fm, close to hot springs. Samples AR14a and b are characterized by mixed layers chlorite-smectite, whereas samples AR12, AR15 and AR30 by mixed layers illite-smectite. In particular, sample AR12 displays two populations of mixed layers I-S. The first population consists of random ordered structures with low illite layers (20%) consistent with data of rocks **affected by syn-folding deformation** and the second population is made up of low expandable long-range ordered I-S with illite contents of 80%. One population of mixed layers I-S occurs in samples AR15 and AR30 with high contents (80%) of illite layers and R3 stacking order (Fig. **6**b).

The occurrence of either mixed layer chlorite-smectite or low expandable I-S indicate the interaction with high temperature geothermal fluids. In fact, in active hydrothermal systems, both subaerial and submarine, the first appearance of mixed layers chlorite-smectite was reported between 150 and 200 °C, and its presence was noted up to temperatures of approximately 300 °C (Schiffman and Fridleifsson 1991; Shau and Peacor 1992). Comparison with temperature models for I-S geothermometry suggests a temperature for the occurrence of long-range ordered I-S of at least 165 °C (Środoń, 1999).

4.3 Organic Matter Optical Microscopy

Reflected light optical microscopy analyses of the Yacoraite Fm. allowed recognizing a prevalence of indigenous fragments of the huminite-vitrinite group macerals and a less abundant population of reworked inertinite fragments. The indigenous vitrinite fragments show reflectance values of about 0.6-0.7% indicating the early-mid mature stage of hydrocarbon generation (Table 1 and Fig. 3a).

4.4 Fluid Inclusion Analyses

Petrographic analyses on double polished wafers mainly show the presence of mono-phase primary inclusions and scarcely healed microfractures with secondary inclusions in all samples (Fig. **7**). This, together with an inhomogeneous distribution of vapour phase in the less abundant two-phase inclusions, suggests an entrapment temperature below 50-60 °C (immiscible liquid and vapour) (Fig. 3; Table 1). Nevertheless, sporadic two-phase fluid inclusion assemblages with homogeneous vapour distribution characterize sample AR12 (Fig. **7**a).

Homogenization temperatures (Th) of 115 °C and ice melting temperatures (Tm) of -0.4-0.8 °C measured in a dozen of inclusions within calcite crystals provide constraints on trapping temperature and fluid salinity, respectively.

Tens of primary and secondary liquid inclusions were observed in sample AR19 within gypsum and calcite crystals confirming an entrapment temperature lower than 50 °C (Fig. **7**b).

5. Burial and thermal modelling

Thermal models were performed for the Anta Yaco area, along the southwestern limb of the Sierra de La Candelaria ridge, far away from the hot springs, in order to define the

maximum burial conditions (Fig. **8**a), and for the Hotel Termas area, in the northern **sector** of the anticline, close to hot springs, in order to unravel the hot fluid contribution to thermal maturity (Fig. **8**c).

The reconstructed burial history for the two investigated areas began in Barremian times with the deposition of the syn-rift deposits of the Pirgua Subgroup (Figs. **8**a and c). During the Cretaceous, sedimentation took place at low sedimentation rates in the basin until the deposition of the Late Cretaceous-early Paleocene post-rift basinal deposits of the Balbuena Subgroup that reached a thickness of 150 m (Marquillas et al., 2005). From the early Paleocene to the lower Eocene, 50 m thick succession of the Santa Bárbara Subgroup sedimented. A hiatus of about 35 Ma in the stratigraphic record occurred from the lower Eocene to the middle Miocene (Reynolds et al., 2000; Del Papa et al., 2010). Deposition started again during middle Miocene times with the syn-orogenic sedimentation of the Metán Subgroup and continued at high sedimentation rates from late Miocene to Zanclean times with the sedimentation of the Jujuy Subgroup rocks (Reynolds et al., 2000). At that time, the sedimentary succession of both areas experienced maximum burial conditions recording paleo-temperatures of about 115 °C for the syn-rift deposits, about 95 °C for the post-rift and 85 °C for the syn-orogenic deposits (Fig. **8**). The syn-rift succession, corresponding to the reservoir of the Rosario de la Frontera geothermal system, experienced a thermal evolution consistent with the early stage of hydrocarbon generation during Miocene times, whereas the siliciclastic syn-orogenic succession acting as cap rock, is in the immature stage of hydrocarbon generation.

In addition, fluid inclusions analyses performed in **NNE-SSW-striking gypsum-filled** veins **and N-S-striking calcite-filled veins** of the **Anta Fm** record entrapment temperatures < 50 °C consistent with the early stage of rift inversion coeval to fold growth (samples AR 17, 19b in Table 1; Fig. 3).

Since the early Pliocene (about 4 Ma ago), the Anta Yaco and Hotel Termas areas experienced different evolutionary history as a result of the inversion of Cretaceous rift related normal faults during the Quechua orogenic phase (Carrapa et al., 2011; Barcelona et al., 2014) which uplifted the two sectors at different rates. Differential uplift triggered erosion that removed about 1,000 m thick succession from the Hotel Termas area to the north of the Sierra de La Candelaria ridge at rates of 0.25 mm/yr (Fig. **8**a) and about 350 m in the Anta Yaco area at rates of 0.09 mm/yr (Fig. 7c). As thermochronometric data are not available for the areas, the reconstructed burial history represents the most conservative scenarios where the sedimentary succession experienced the minimum time

of burial with the onset of exhumation in early Pliocene times. The simplified burial and thermal models allow an acceptable calibration against mixed layer I-S and vitrinite reflectance data, as indicated by the present-day maturity curve of figures **8b** and **8d** suggesting that levels of thermal maturity are ruled by sedimentary burial.

Furthermore, we point out that the present-day maturity curve fits paleothermal indicators also considering the onset of exhumation during Quaternary times as suggested by Seggiaro et al. (2015).

The conductive thermal model performed in the Hotel Termas area (Fig. **8d**), displays the scarce fitting of the present-day maturity curve with paleothermal indicators derived from highly fractured rocks. In this case, the occurrence of long-range ordered mixed layer I-S indicates a temperature of at least 165 °C (Środoń, 1999) as a result of interaction of high temperature geothermal fluids circulating in highly fractured rocks. In addition, fluid inclusions analyses on calcite extensional veins of highly fractured rocks, indicate an entrapment temperature of about 115 °C consistent with the present-day temperature of thermal fluids at depths of 2,000 m that are in the range of 100-130 °C (Seggiaro et al., 1995; Chiodi et al., 2015). These paleofluid temperatures are higher than those currently measured at surface (71-81 °C, Fig.3) in thermal springs of the Hotel Termas area where a fluid mixing with shallow depth aquifer can be neglected (Chiodi et al., 2015). This evidence allows **us to suggest** that fluid temperature of the geothermal system probably decreased through time and space (moving from depth toward to the surface).

These pieces of evidence suggest that deformation related to NNW-SSE oblique faults may have focused hot fluids migration triggering heat convection and localized thermal alteration of the cap rock (Fig. **9**). On the other hand, fractures developed during the early and the intermediate stages of rift inversion, mainly coeval with fold growth, were not affected by thermal alteration suggesting that they did not act as fluid pathways.

6. Discussion and conclusion

The analyses of the cap rock fracture patterns and the definition of levels of thermal maturity of the basin allowed us to distinguish the thermal fingerprint associated to sedimentary burial from that related to fluid migration, and to trace the main pathways of hot fluids. As a result, we identified two quality categories **for** the cap rock: **(1) rocks acting as good insulators deformed during the initial stage of anticline growth and (2) rocks acting as bad insulators deformed by late transpressive kinematics.**

Cap rocks **with syn-folding features** are mainly characterized by low levels of thermal alteration (low contents of illite layers in mixed layers I-S and vitirinite reflectance values of about 0.6-0.7%) and by homogenization temperatures of fluid inclusions of about 50 °C which were experienced during sedimentary burial and early stage of folding. In particular, the thermal fingerprint of the basin is associated to a progressive increase of the illite content in mixed layer I-S as a function of stratigraphic age. Mixed layers I-S evolve from random ordered structures typical of syn-orogenic deposits (Anta, Jesús Maria Fms) to short-range ordered (R1) structures occurring in the syn-rift deposits of the Pirgua Subgroup. This evidence is valid for several localities across the regional anticline where fracture patterns has not enhanced rock permeability.

On the contrary, **post-folding fractured** rocks are characterized by high levels of thermal alteration indicated by low expandability mixed layer I-S and R3 stacking order and by microthermometric analysis of fluid inclusions on calcite veins, which record homogenization temperatures of about 115 °C. Temperature-dependent clay minerals and fluid inclusions suggest a strong water-rock interaction consistent with hot fluids circulation.

These results indicate that the cap rock of the Rosario de La Frontera geothermal system regionally acts as a good thermal insulator since low levels of thermal alteration are ubiquitous along the structure where rocks are poorly deformed but locally fails as NNW-SSE fractures enhanced secondary permeability driving hot fluids circulation.

In this paper, we improve the model of geothermal fluid circulation proposed by Chiodi et al. (2015) and Maffucci et al. (2015) showing the primary role of fault and fracture systems as pathways of hot fluids from the deep reservoir toward the surface (Fig. **9**).

The geothermal system of Rosario de La Frontera is mainly recharged by meteoric water that infiltrates in the central **sector** of the anticline where fractured sandstones of the syn-rift deposits (Pirgua Subgroup) crop out. Recharging meteoric waters circulate within the reservoir rocks and move to the north assisted by primary and secondary reservoir permeability. In the northern area of the anticline (Hotel Termas area), where the reservoir is located at depths higher than 2,000 m, fluids **have** an average temperature of about 115 °C, as indicated by silica geothermometers (**Chiodi et al., 2015**). In this framework, **we highlight the major role of deep-seated** NNW-SSE oblique fault planes **and fracture patterns related to the late transpression kinematics that allowed meteoric fluids to reach high depths, to let them heat up, and triggering their** upflow toward the surface. As a result, in proximity of the northern plunge of the ridge, close to the Hotel Termas spa,

several hot springs occur **in the proximity** of low permeability syn-orogenic deposits of the cap rock (Anta Fm).

The mid-enthalpy geothermal system of Rosario de La Frontera can be used as a pilot study for understanding fluids circulation in other geothermal systems associated to inverted structures in the Subandean foreland fold-and-thrust belt.

In conclusion, the study of thermal maturity of cap rocks has shown how compositional and structural changes in mixed layers I-S and homogenization temperatures of fluid inclusions are function of fluid temperature and fractures distribution. We propose that this approach may turn out to be useful in areas of geothermal interest where either subsurface data are scarce or surface thermal anomalies are lacking (e.g., blind geothermal systems).

Acknowledgements

We acknowledge W. Báez, P. Caffe, P. Pierantoni, J. Viramonte as CUIA project colleagues, for precious support in the field and interesting discussions on Andean geology and geothermal energy issues. Thanks are also due to Seggiaro for priceless suggestions, D. Santarelli for logistic support in Buenos Aires and Sergio Lo Mastro for XRD facilities in Roma Tre labs. Fundings: Project Miur-CUIA 2010 (coordinator C. Invernizzi); Miur-PhD Fondo Giovani to R. Maffucci; “Roma Tre” (responsible S. Corrado and G. Giordano) and “Sapienza” (responsible S. Bigi) University research fundings.

References

Aldega, L., Botti, F., Corrado, S., 2007. Clay mineral assemblages and vitrinite reflectance in the Laga Basin (Central Appenines, Italy): What do they record? Clays and Clay Minerals, 55 (5), 504-518.

Allmendinger, R. W., Ramos, V. A., Jordan, T. E., Palma, M. and Isacks, B. L., 1983. Paleogeography and Andean structural geometry, northwest Argentina. Tectonics 2, 1-16.

Barcelona, H., Favetto, Al., Peri, V.,, Pomposiello, C.,, Ungarelli, C. 2013. The potential of audiomagnetotellurics in the study of geothermal fields: A case study from the northern segment of the La Candelaria Range, northwestern Argentina. Journal of Applied Geophysics, 88, 83-93.

Barcelona, H., Peri, G., Tobal, J., Sagripanti, L., Favetto, A., 2014. Tectonic activity revealed by morphostructural analysis: Development of the Sierra de la Candelaria range, northwestern Argentina. Journal of South American Earth Sciences 56, 376-395.

Barton, C. A., Hickman, S., Morin, R., Zoback, M. D., Finkbeiner, T., Sass, J., Benoit, D., 1997. Fracture permeability and its relationship to in-situ stress in the Dixie Valley, Nevada, geothermal reservoir. Proceedings. Twenty-Second Workshop on Geothermal Reservoir Engineenng Stanford Unlverslty, Stanford. California, January 27-29, 1997, SGP-TR- 155.

Basin Mod® 1-D for WindowsTM, 1996. A Basin Analysis Modelling System version 5.4 Software: Denver, Platte River Associates, 386 p.

Bonaparte, J., Salfity, J., Bossi,G.& Powell,J., 1977. Hallazgo de dinosaurios y aves cretacicas en la Formación Lecho de El Brete (Salta), próximo al lÍmite con Tucumán. Acta Geológica Lilloana, 14, 5–17.

Bossi, G.E., 1969. GeologÍa y estratigrafÍa del sector sur del Valle de Choromoro. Acta Geol Lilloana 10, 17–64.

Bustin, R.M., Barnes, M.A., and Barnes, W.C., 1990. Determining levels of organic diagenesis in sediments and fossil fuels, in McIleareath, I.A., and Morrow, D.W., eds., Diagenesis: Geoscience Canada Reprint, 4th series, 205-226.

Butler, R. W. H., 1992. Hydrocarbon maturation, migration and tectonic loading in the Western Alps, in England, W. A., and Fleet, A.J., eds., Petroleum migration: Geological Society of London Special Publication, 59, 227-244.

Carapezza M. L., Ranaldi M., Gattuso A., Pagliuca N. M., Tarchini L., 2015. The sealing capacity of the cap rock above the Torre Alfina geothermal reservoir (Central Italy) revealed by soil CO_2 flux investigations. Journal of Volcanology and Geothermal Research, 291, 25–34.

Caricchi, C., Aldega, L., Corrado, S., 2015. Reconstruction of maximum burial along the Northern Apennines thrust wedge (Italy) by indicators of thermal exposure and modeling. Geological Society of America Bulletin, doi:10.1130/B30947.1

Carrapa, B., Trimble, J., Stockli, D., 2011. Patterns and timing of exhumation and deformation in the Eastern Cordillera of NW Argentina revealed by (U-Th)/He thermochronology. Tectonics 30, TC 3003 doi:10.1029/2010TC002707.

Carrera, N., Muñoz, J.A., Sábat, F., Mon, R., Roca, E., 2006. The role of inversion tectonics in the structure of the Cordillera Oriental (NW Argentinean Andes). J. Struct. Geol. 28 (11), 1921–1932. http://dx.doi.org/10.1016/j.jsg.2006.07.006.

Chiodi, A., Tassi, F., Baez, W., Maffucci, R., Di Paolo, L., Viramonte, J.G., 2012a. Características geoquímicas e isotópicas de los fluidos hidrotermales del sistema geotérmico de Rosario de la Frontera, Sierra de la Candelaria, Salta, Argentina. In: Congreso Latinoamericano de Hidrogeología y IV Congreso Colombiano de Hidrogeología. Colombia.

Chiodi, A., Tassi, F., Baez, W., Maffucci, R., Di Paolo, L., Viramonte, J.G., 2012b. Chemical and isotope characteristics of the Rosario de la Frontera geothermal fluids, La Candelaria Range (Salta, Argentina). 86° Convegno SGI, Arcavacata di Rende-Cosenza, 18-20 Settembre. Rend. Online Soc. Geol. It. ISSN: 2035-800821, 800-801.

Chiodi A., Tassi, F., Báez, W., Maffucci, R., Invernizzi, C., Giordano, G., Corrado, S., Bicocchi, G., Vaselli, O., Viramonte, J.G., Pierantoni, P.P., 2015. New geochemical and isotopic insights to evaluate the geothermal resource of the hydrothermal system of Rosario de la Frontera (Salta, northern Argentina). Journal of Volcanology and Geothermal Research, 295, 16-25.

Corrado, S., Invernizzi, C., Aldega, L., D'Errico, M., di Leo, P., Mazzoli, S., Zattin, M., 2010. Testing the validity of organic and inorganic thermal indicators in different tectonic settings from continental subduction to collision: The case history of the Calabria-Lucania border (southern Apennines, Italy). Journal of the Geological Society, 167 (5), pp. 985-999.

Corrado S., Aldega L., Celano A. S., De Benedetti A. A., Giordano G., 2014. Cap rock efficiency and fluid circulation of natural hydrothermal systems by means of XRD on clay minerals (Sutri, Northern Latium,Italy). Geothermics, 50, 180– 188, http://dx.doi.org/10.1016/j.geothermics.2013.09.011

Cristallini, E., Cominguez, A.H. y Ramos, V.A., 1997. Deep structure of the Metán–Guachipas region: tectonic inversion in northwestern Argentina. Journal of South American Earth Sciences, 10, 403-421.

Del Papa, C., Kirschbaum, A., Powell, J., Brod, A., Hongn, F., Pimentel, M., 2010. Sedimentological, geochemical and paleontological insights applied to conti- nental omission surfaces: a new approach for reconstructing an Eocene fore- land basin in NW Argentina. Journal of South American Earth Sciences 29, 327-345.

Diamond, L.W., 2003. Glossary: terms and symbols used in fluid inclusions studies. In: Samson, I., Anderson, A.,Marshall, D. (Eds.), Fluid Inclusions: Analysis and Interpretation. Short Course Series, vol.32. Mineralogical Association of Canada, pp. 363–372.

Di Paolo, L., Aldega, L., Corrado, S., Giordano, G., Invernizzi, C., 2012. Modelling of organic and inorganic paleo-thermal indicators to constrain the evolution of the geothermal system of Rosario de La Frontera (La Candelaria Ridge, NWArgentina): a new tool for geothermal exploration. Rend. Online Soc. Geol. Ital. 21, 807–808.

Dobson P.F., Kneafsey T.J., Hulenb J., Simmons A., 2003. Porosity, permeability, and fluid flow in the Yellowstone geothermal system, Wyoming. Journal of Volcanology and Geothermal Research, 123, 3–4, 313–324. doi:10.1016/S0377-0273(03)00039-8

Ghassemi, A., 2012. A review of some rock mechanics issues in geothermal reservoir development (Review). Geotechnical and Geological Engineering, 30, 3, 2012, 647-664.

Giordano G., Pinton, A., Cianfarra, P., Baez, W., Chiodi, A., Viramonte J., Norini, G, Groppelli G., 2013. Structural control on geothermal circulation in the Cerro Tuzgle–Tocomar geothermal volcanic area (Puna plateau, Argentina). Journal of Volcanology and Geothermal Research, 249, 77–94

Gómez Omil, R.J., Boll, A., Hernández, R.M., 1989. Cuenca cretácico- terciaria del Noroeste argentino (Grupo Salta). In: Chebli GA, Spalletti LA (eds) Cuencas Sedimentarias Argentinas. Universidad Nacional de Tucumán, Serie de Correlación Geológica 6, 43–64.

González, O., Viruel, M., Mon, R., Tchilinguirian, P., Barber, E., 2000. Hoja Geológica 2766-II. San Miguel de Tucumán. Boletín 245. Programa Nacional de Cartas Geológicas, 1:250.000. SEGEMAR.

Hain, M.P., Strecker, M.R., Bookhagen, B., Alonso, R.N., Pingel, H., Schmitt, A.K., 2011. Neogene to Quaternary broken foreland formation and sedimentation dynamics in the Andes of NW Argentina (25°S). Tectonics 30, 1-27.

Iaffa, D.N., Sàbat, F., Muñoz, J.A., Mon, R., Gutierrez, A.A, 2011. The role of inherited structures in a foreland basin evolution. The Metán Basin in NW Argentina. Journal of Structural Geology 33, 1816-1828.

Iaffa, D.N., Sabat, F., Munoz, J.A., Carrera N., 2013. Basin fragmentation controlled by tectonic inversion and basement uplift in Sierras Pampeanas and Santa Barbára System, northwest Argentina. Geological Society, London, Special Publications, 377.

Invernizzi, C., Pierantoni, P., Chiodi A., Maffucci, R., Corrado, S., Baez, W., Tassi, F., Giordano G., Viramonte, J., 2014. Preliminary assessment of the geothermal potential of Rosario de la Frontera area (Salta, NW Argentina): insight from hydro-geological, hydro-geochemical and structural investigations. Journal of South American Earth Science, 54, 20-36.

Jagodzinski, H., 1949. Eindimensionale Fehlordnung in Kristallen und ihr Einfluss auf die Röntgen Interferenzen. Acta Crystallographica, 2, 201-207.

Jordan, T. E., Isacks, B., Ramos,V.A.& Allmendin- ger, R. W. 1983. Mountain building in the Central Andes. Episodes, 3, 20–26.

Jordan, T. E., and R. W. Allmendinger, 1986. The Sierras Pampeanas of Argentina: A modern analogue of Rocky Mountain foreland deformation, Am. J. Sci., 286, 737 –764.

Kley, J., C. R. Monaldi, and J. A. Salfity, 1999. Along- strike segmentation of the Andean foreland: Causes and consequences, Tectonophysics, 301, 75–94.

Kley, J., Monaldi, C.R., 2002. Tectonic inversion in the Santa Barbara System of the central Andean foreland thrust belt, northwestern Argentina. Tectonics 21(6), 1061.

Maffucci, R., Bigi, S., Chiodi, A., Corrado, S., Di Paolo, L., Giordano, G., 2012. Fracture Modeling applied to the geothermal system potential reservoir of Rosario de La Frontera (La Candelaria Ridge, NW Argentina). Rend. Online Soc. Geol. It. 21, 829-831.

Maffucci R., Bigi S., Corrado S., Giordano G., Chiodi A., Di Paolo L., 2013. Reconstruction of a “Discrete Fracture Network” in the geothermal reservoir of Rosario de La Frontera (La Candelaria Ridge, Salta province, NW Argentina). European Geothermal Congress 2013 Extended Abstract Pisa, Italy, 3-7 June 2013.

Maffucci, R., Bigi, S., Corrado, S., Chiodi, A., Di Paolo, L., Giordano, G., Invernizzi, C., 2015. Quality assessment of reservoirs by means of outcrop data and "discrete fracture

network" models: the case history of Rosario de La Frontera (NW Argentina) geothermal system. Tectonophysics, 647-648, 112-131.

Marrett, R.A., Allmendinger, R.W., Alonso, R.N., Drake, R.E., 1994. Late Cenozoic tectonic evolution of the Puna Plateau and adjacent foreland, northwestern Argentine Andes. J. S. Am. Earth Sci. 7, 179–207.

Marquillas, R., Del Papa, C., Sabino, I.F., 2005. Sedimentary aspects and paleoenvironmental evolution of a rift basin: Salta Group (Cretaceous-Paleogene), northwestern Argentina. International Journal of Earth Sciences 94, 94-113.

Merriman, R.J., and Frey, M., 1999. Patterns of very low-grade metamorphism in metapelitic rocks, in Frey, M., and Robinson, D., eds., Low grade metamorphism: Oxford, Blackwell, 61-107.

Moore, D.M., and Reynolds, R.C., Jr., 1997. X-Ray diffraction and the identification and analysis of clay minerals: Oxford, Oxford University Press, 1-378.

Moreno, J. A. 1970. Estratigrafía y paleogeografía del Cretácico Superior en la cuenca del Noroeste Argentino, con especial mención de los Subgrupos Balbuena y Santa Bárbara. Revista Asociación Geológica Argentina, 24, 9–44.

Moreno Espelta, C., Viramonte, J.G., Arias, J.E., 1975. Geología del área termal de Rosario de la Frontera y sus posibilidades geotérmicas. Actas del II Congreso Ibero-Americano de Geología Económica IV, pp. 543–548.

Müller, C., Siegesmund, S., and Blum, P., 2010. Evaluation of the representative elementary volume (REV) of a fractured geothermal sandstone reservoir. Environmental Earth Sciences. DOI:10.1007/s12665-010-0485-7

Pesce A. & Miranda F., 2003. Catálogo de manifestaciones termales de la República Argentina. Volumen I – Región Noroeste. SEGEMAR. Buenos Aires. Argentina.

Phillip, S. L., 2015. Fault zones and associated fracture systems in geothermal reservoir rocks. AAPG Europe Conference, Catania, Sicily, 16-17th April, 2015.

Rahman, M.M.a , Rahman, S.S., 2013. Studies of hydraulic fracture-propagation behavior in presence of natural fractures: Fully coupled fractured-reservoir modeling in poroelastic environments. International Journal of Geomechanics, 13, 6, 809-826

Ramos, V.A., 1999. Las provincias geológica del territorio argentino. In: Caminos, R. (ed.) Geológia Argentina. Instituto de Geologia y Recursos Minerales, Buenos Aires, Anales, 29, 41-96.

Ramos, V.A., 2008. The basement of the Central Andes: the Arequipa and related terranes. Annu. Rev. Earth Planet. Sci. 36, 289-324.

Reyes, F.C., Salfity, J.A., 1973. Consideraciones sobre la estratigrafia del Cretacico (Subgrupo Pirgua) del noroeste Argentino. In: V Congreso Geologico Argentino, vol. 2, pp. 355-385.

Reynolds, J.H., Galli, C.I., Hernández, R.M., Idleman, B.D., Kotila, J.M., Hilliard, R.V., Naeser, C.W., 2000. Middle Miocene tectonic development of the Transition Zone Salta Province, northwest Argentina: magnetic stratigraphy from the Metán Subgroup, Sierra de González. GSA Bulletin 112 (11).

Rossetti F., Aldega L., Tecce F., Balsamo F., Billi, A. & Brilli M. (2011). Fluid flow within the damage zone of the Boccheggiano extensional fault (Larderello-Travale geothermal field, central Italy): structures, alteration and implications for hydrothermal mineralization in extensional settings. Geological Magazine, 148 (4), 558-579.

Russo, A., Serraiotto, A., 1979. Contribución al conocimiento de la estratigrafía terciaria en el noroeste argentino. VII Congreso Geológico Argentino, Neuquén (1978), Actas 1, 715-730.

Salfity, J.A.& Marquillas, R. A. 1981. Las unidades estratigráficas cretácicas del Norte de la Argentina. In: Volkheimer,W.& Musacchio, E. (eds) Cuencas Sedimentarias del Jurásico y Cretácico de América del Sur, 1. Comité Sudamericano del Jurásico y Cretácico, Buenos Aires, Argentina, 303–317.

Salfity, J.A., Monaldi, C.R., Marquillas, R.A., Gonzales, R.E., 1993. La Inversion Tectonica del Umbral delos Gallos en la cuenca del Grupo Salta durante la Fase Incaica. In: Actas del XII Congreso Geologico Argentino y II Congreso de Exploracion de Hidrocarburos, Asoc. Geol. Argent., Mendoza, Argentina.

Salfity, J.A., Monaldi, C., 2006. Hoja Geológica 2566 - IV Metán. Boletín 319. Programa Nacional de Cartas Geológicas, 1:250.000. SEGEMAR.

Schiffman P, Fridleifsson GO. 1991. The smectite to chlorite transition in Drillhole NJ-15, Nesjavellir Geothermal Field, Iceland: XRD, BSE and electron microprobe investigations. J. Metamorph. Geol. 9:679–96.

Sclater, J.G., and Christie, P.A.F., 1980. Continental stretching: an explanation of post-Mid Cretaceous subsidence on the Central North Sea Basin: Journal of Geophysical Research, 85, 3711-3739.

Seggiaro, R., Aguilera, N., Gallardo, E., Ferreti, J., 1995. Structure and geotermal potential of the Rosario de la Frontera termal área. Salta. Argentina. World Geothermal Congress. Florence. Italy, 2, 764-767.

Seggiaro, R., Aguilera, N., Ferretti, J., Gallardo, E., 1997. Estructura del area geotermica de Rosario de la Frontera, Salta, Argentina. VIII Congreso Geologico Chileno. Actas, 1 (2), 390-394 Antofagasta.

Seggiaro, R., Gallardo, E., Aguilera, N., Vitulli, N., Brandan, E., Bercheñi, V., Barrabino, E., Celedon, M., Villagran, A., 2015. Structural model of the Sierra la Candelaria thermal area, department of Rosario de la Frontera, Salta._Revista de la Asociacion Geologica Argentina, 72(2).

Shau YH, Peacor DR. 1992. Phyllosilicates in hydrothermally altered basalts from DSDP Hole 504B, Leg 83—a TEM and AEM study. Contrib. Mineral. Petrol. 112:119–33.

Stearns, D.W., 1968. Certain aspect of fracture in naturally deformed rocks. In: Rieker, R.E. (Ed.), National Science Foundation Advanced Science Seminar in Rock Mechanics, Special report. Air Force Cambridge Research Laboratories, Bedford, MA, pp. 97–118.

Środoń J., 1999. Nature of mixed-layer clays and mechanisms of their formation and alteration. Annu. Rev. Earth Planet. Sci. 27:19–53.

Sweeney, J.J., and Burnham, A.K., 1990. Evaluation of a simple model of vitrinite reflectance based on chemical kinetics: American Association of Petroleum Geologists Bulletin, 74, 1559-1570.

Todesco, M. & Giordano, G., 2010. Modelling of CO_2 circulation in the Colli Albani area. In: Funiciello, R. & Giordano, G. (eds) The Colli Albani Volcano. Geological Society, London, Special Publications of IAVCEI, 3, 311–328

Timlin, M., 2009. Effects of stratigraphy on geothermal reservoir performance. In: AAPG Annual Convention and Exhibition, Denver, CO, USA, 7-10.06.2009.

Turner, J.C.M., 1959. Estratigrafía del cordón de Escaya y de la sierra de Rinconada (Jujuy). Rev Asoc Geol Arg 13, 15-39.

Vignaroli, G., Aldega, L., Balsamo, F., Billi, A., De Benedetti, A. A., De Filippis, L., Giordano, G., Rossetti, F., **2015**. A way to hydrothermal paroxysm, Colli Albani volcano, Italy. GSA Bulletin, 127 (5/6), 672-687. doi: 10.1130/B31139.1.

Wang, X., Ghassemi, A., 2011. A three-dimensional stochastic fracture network model for geothermal reservoir stimulation. Proceedings, Thirty-Sixth Workshop on Geothermal Reservoir Engineering Standford University, Standford, California, Janaury 31 – Febraury 2, 2011.

Figure and table captions

Fig. 1 Location of the study area (**modified after** Chiodi et al., 2015).

Fig. 2 (a) Geological map of Sierra de La Candelaria anticline (modified after Maffucci et al., 2015). (b) Chronostratigraphic scheme showing the main tectonic events controlling the deposition of the litostratigraphic units (redrawn after Carrera et al., 2006).

Fig. 3 a) Sketch map showing sampling location and analytical results from inorganic and organic thermal indicators. Stacking order and illite content of mixed layers I-S, vitrinite reflectance and related standard deviation, and homogenization and melting temperatures of fluid inclusions are indicated in the boxes. Outlet temperatures of thermal springs collected in April 2012 are also reported (Invernizzi et al., 2014) b) Stratigraphic column

showing the sampled stratigraphic units. For each one, the type of deposit and the related stacking order are also **indicated**. FHS and CHS indicates samples collected far away and close to hot springs, respectively.

Fig. 4 Brittle deformation observed in the **Anta Yaco area, far away from the** hot springs, **and stereographic projections (Schmidt net, lower hemisphere) of the collected structural data: E-W systematic fracture set occurring in the Pirgua Subgroup (a) and Yacoraite Fm (b). (c) stereographic projection showing the NNW–SSE- and E–W-striking conjugate system of fractures in the Anta Fm.**

Fig. 5 Examples of the structural discontinuities observed in the strata **of the Anta Fm, in the Hotel Termas area, close to hot springs, and related stereographic projections (Schmidt net, lower hemisphere):** (a) NNE-SSW-striking gypsum extensional veins related to fold growth. (b) Strike-slip sub-vertical fault plane **striking N40°W** with a left-lateral sense of shear. A small pull-apart is formed by extension between the overlapping fault surfaces. (c) Small normal faults dipping to N150°. (d) **Stereographic projections of structural data (veins, fractures and faults).**

Fig. **6** Selected XRD patterns of the <2 µm oriented mounts observed in samples collected from (a) **syn-folding** fractured rocks, far away **from** the hot springs (sample AR11) and (b) **post-folding** fractured rocks, close to hot springs (sample AR30).

Fig. **7** Fluid inclusions data **for the Anta Formation close to hot springs**. Microphotograph**s** show primary and secondary inclusions: (a) secondary two-phase inclusions **from post-folding calcite veins** (sample AR12); (b) primary mono-phase inclusions **from syn-folding gypsum veins** (sample AR19). **Arrows indicate selected inclusions for microthermometric analysis. In (b) the circled area includes a primary fluid inclusion assemblage.**

Fig. **8** Representative one-dimensional burial and thermal models of the Sierra de La Candelaria stratigraphic succession performed (a) far away (Anta Yaco area) and (c) close to hot springs (Hotel Termas area) with an inset of the last 20 Ma. (b) and (d): depth vs maturity plot constrained by mixed layers I-S and vitrinite reflectance data. Acronyms: K-Cretaceous; Pal-Paleocene; E-Eocene; O-Oligocene; M-Miocene; P-Pliocene; Q-Quaternary.

Fig. **9** Three-dimensional conceptual model of the underground fluid circulation of Rosario de La Frontera geothermal system (redrawn and modified from Chiodi et al., 2015). In the northern area of the Termas anticline, **fracture patterns** formed during fold growth (black) and the late transpression that took place along the late NNW-SSE fault plane (red) **are shown** . The latter **fracture pattern** represents the preferential pathway of hot fluids from the reservoir toward to the surface.

Table 1: Summary of inorganic and organic thermal parameters and X-ray diffraction (XRD) **semi-**quantitative analysis.

Age	Subgroup	Formation	Location and type of deposit	Samples	Coordinate (Latitude; Longitude)	XRD analysis		%I in I-S (R)	R_o%*	FI	
						<2µm	Whole-rock			Th (°C)	Tm (°C)
Miocene	Metán	Jesús María	FHS Syn-folding fractured rocks	AR18	25.8263; 64.8916	I_7I-$S_{91}Ch_2$	$Qtz_{12}Cal_4Plg_{10}Hem_2Ph_{72}$	20 (R0)			
		Anta	CHS Syn-folding fractured rocks	AR19a	25.8344; 64.9372	$I_{91}I$-S_5Ch_1	$Qtz_4Cal_1Kfs_1Plg_4Anl_1Ph_{70}Ank_{19}$	20 (R0)			
				AR19b	25.8344; 64.9372	ND	$Cal_{16}Gyp_{84}$			<50°**	
				AR16	25.8391; 64.93268	$I_{29}I$-$S_{70}Ch_1$	$Qtz_7Kfs_1Plg_5Hem_2Ph_{85}$	25 (R0)			
				AR17	25.8396; 64.93123	$I_{20}I$-S_{80}	$Qtz_{16}Kfs_1Plg_5Anl_3Hem_2Ph_{75}$	20 (R0)		<50°/60°**	
				AR21	25.8422; 64.92803	$I_{79}I$-S_{21}	ND	30 (R0)			
				AR1a	25.84535; 64.92992	$I_{17}I$-S_{83}	$Qtz_{16}Kfs_2Plg_3Anl_4Ph_{75}$	20 (R0)			
				AR1b	25.84535; 64.92993	$I_{25}I$-S_{75}	$Qtz_2Cal_1Kfs_2Plg_6Anl_7Py_3Ph_{79}$	20 (R0)			
			CHS Post-folding fractured rocks	AR14a	25.8369; 64.93361	$I_{19}C$-S_{81}	$Qtz_5Cal_{13}Kfs_1Plg_7Anl_3Ph_{71}$			<50°**	
				AR14b	25.8364; 64.93255	$I_{27}C$-$S_{72}Ch_1$	$Qtz_{18}Cal_2Dol_3Kfs_2Plg_{20}Anl_7Ph_{48}$				
				AR12	25.8386; 64.9316	$I_{36}I$-S_{64}	Qtz_{10} $Dol_1Plg_{10}Ph_{79}$	20 (R0) + 80 (R3)		115°	-0.4°/-0.8°
				AR15a	25.8387; 64.93042	ND	$Qtz_7Kfs_1Plg_2Hem_3Ph_{87}$	ND			
				AR15b	25.8387; 64.93043	$I_{42}I$-S_{57}	$Qtz_{14}Plg_4Anl_1Ph_{81}$	80 (R3)		<50°/70°**	
				AR 30	25.8422; 64.93282	$I_{81}I$-S_{19}	ND	80 (R3)			
			FHS Syn-folding fractured rocks	AR11	25.979; 64.93317	$I_{32}I$-$S_{67}Ch_1$	$Qtz_7Kfs_2Plg_{23}Ph_{68}$	25 (R0)			
				AR 29	25.97931; 64.93237	$I_{85}I$-S_5Ch_{10}	ND	50 (R0)	Barren		
Cretaceous	Balbuena	Yacoraite	FHS Syn-folding fractured rocks	AR10	25.987858; 64.923046	$I_{69}I$-S_{31}	$Qtz_5Cal_1Kfs_1Plg_7Anl_1Py_1Ph_{84}$	20 (R0)			
				AR9	25.987858; 64.923046	ND	ND		0.59 (±0.08; 15)		
				AR8	25.989040; 64.22885	ND	ND		0.67 (±0.11; 19)		

				AR7a	25.9906; 64.9212	$I_{14}I\text{-}S_{86}$	$Qtz_4Kfs_1Plg_9Anl_3Ph_{83}$	20 (R0)	0.65 (±0.11; 13)
				AR7b	25.9906; 64.9213	$I_{16}I\text{-}S_{84}$	$Qtz_3Kfs_1Plg_5Lm_2Ph_{89}$	20 (R0) + 83 (R3)	Barren
				AR5	25.9903; 64.92046	$I_{21}I\text{-}S_{79}$	$Qtz_8Kfs_2Plg_{12}Hem_5Ph_{73}$	20 (R0)	Barren
Pirgua	Los Blanquitos	FHS Syn-folding fractured rocks		AR 27	25.98804; 64.91776	$I_{80}I\text{-}S_{20}$	ND	20 (R0) + 75 (R1)	

Note: Ank-Ankerite; Anl-analcime; Cal-calcite; Ch-chlorite; C-S-mixed-layer chlorite-smectite; Dol-dolomite; Gyp-Gypsum; Hem-hematite; I-illite; I-S-mixed-layer illite-smectite; Lm-laumontite; Kfs-K-feldspar; Ph-phyllosilicates; Plg- Plagioclase; Py-Pyrite; Qtz-quartz; Subscript numbers correspond to mineral weight percentage. FHS= far away hot springs; CHS= close to hot springs; %I in I-S= illite content in mixed layers illite-smectite; R = mixed layer illite-smectite stacking order; Ro%*= in brackets standard deviation and number of reflectance measurements per sample; F.I. = fluid inclusions; Th= homogenization temperature; Tm= ice melting temperature; **= temperature of homogenization estimated from petrographic analyses.

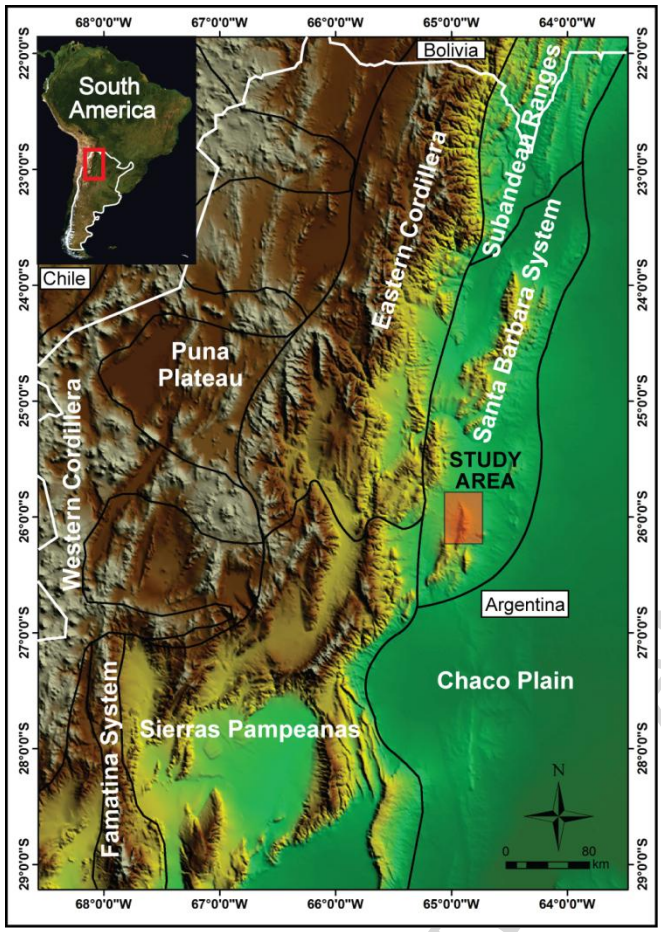

Figure 1

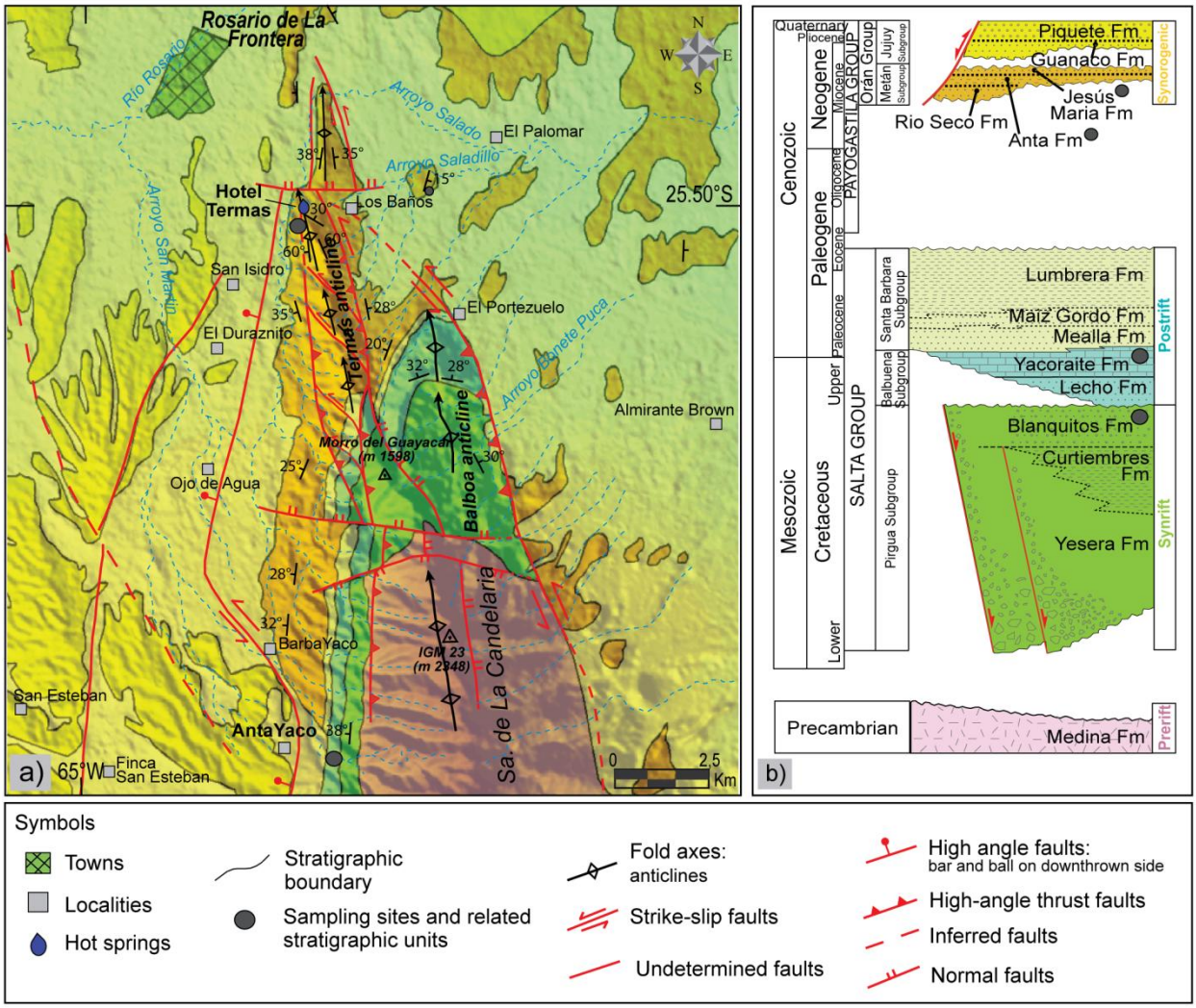

Figure 2

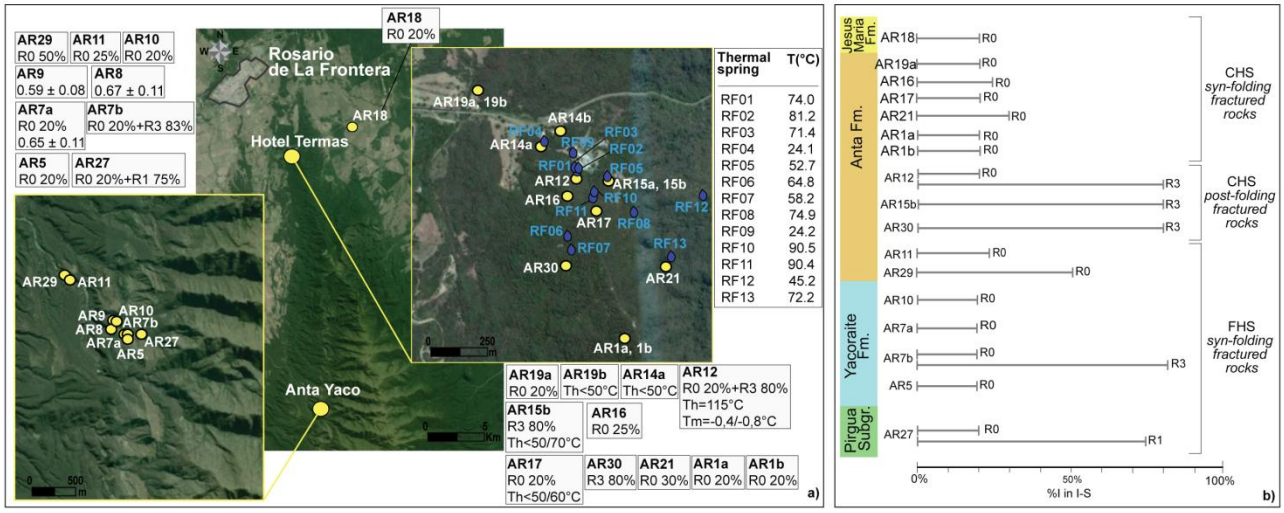

Figure 3

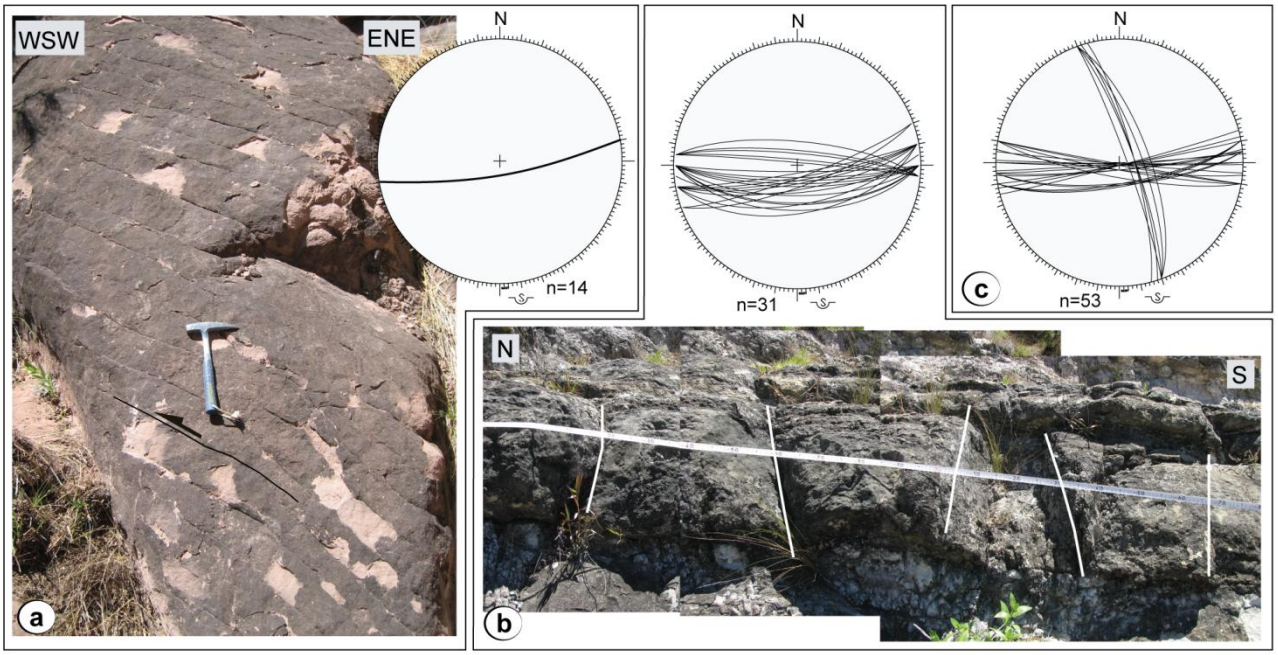

Figure 4

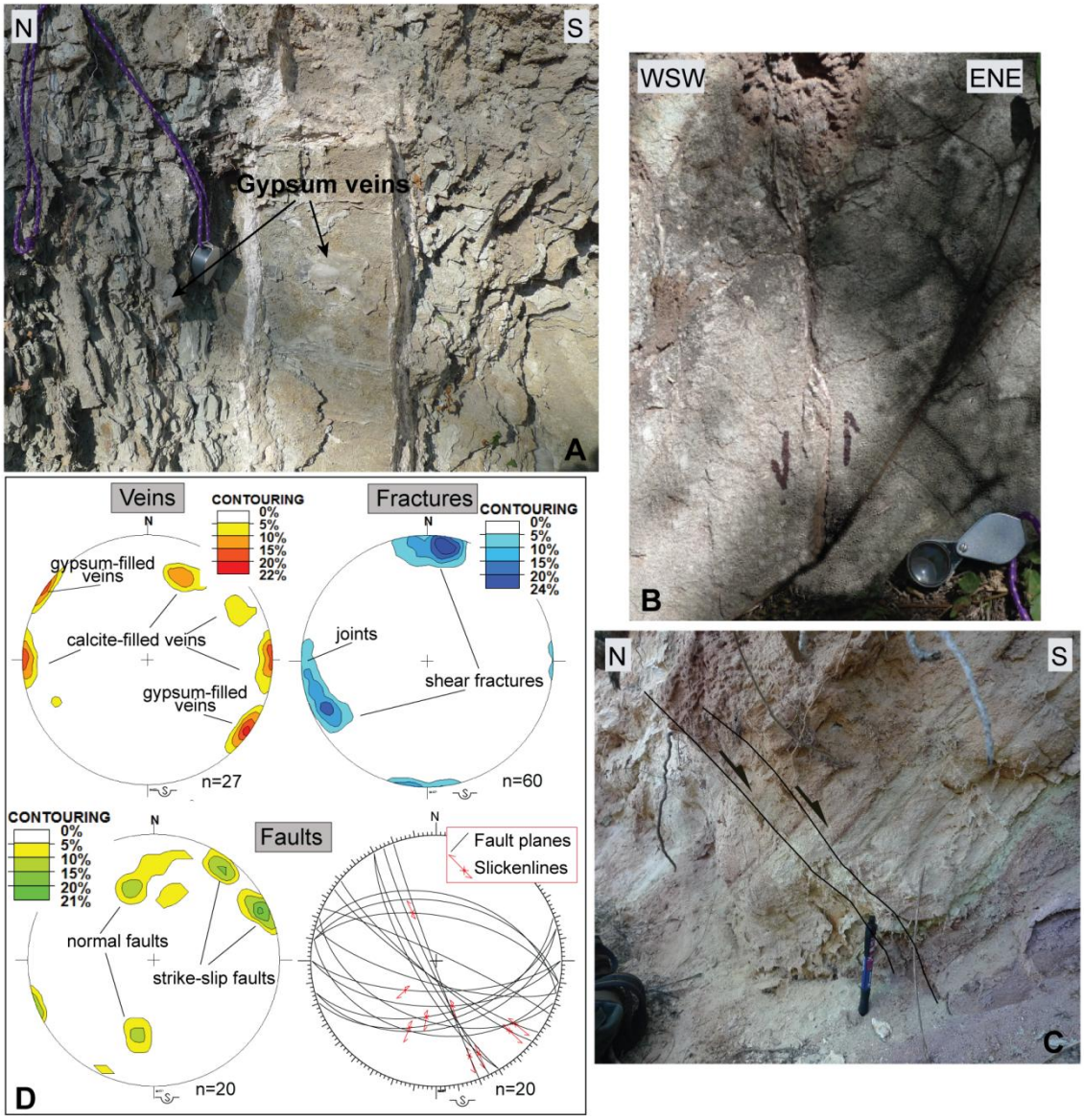

Figure 5

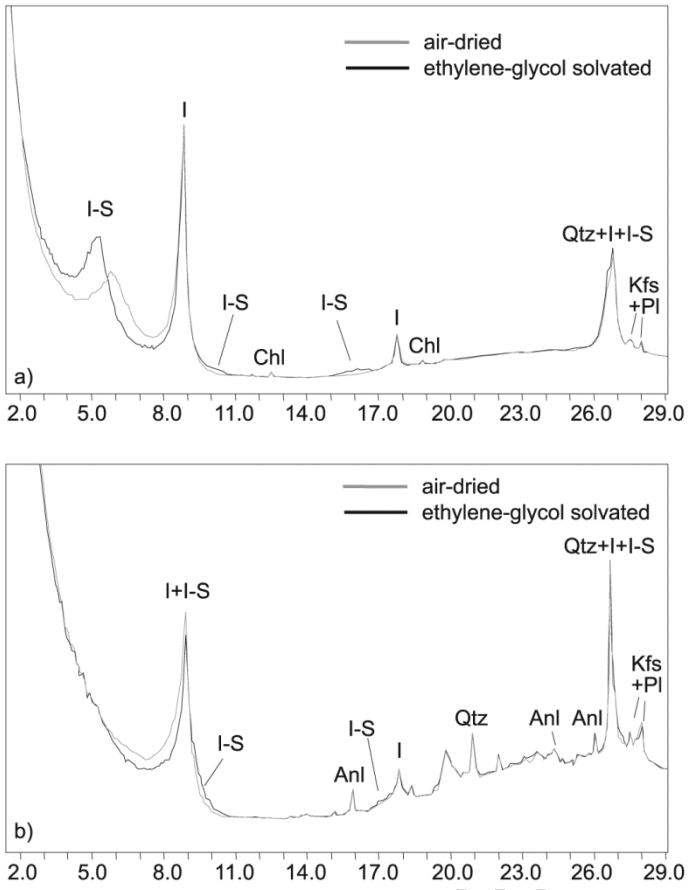

Figure 6

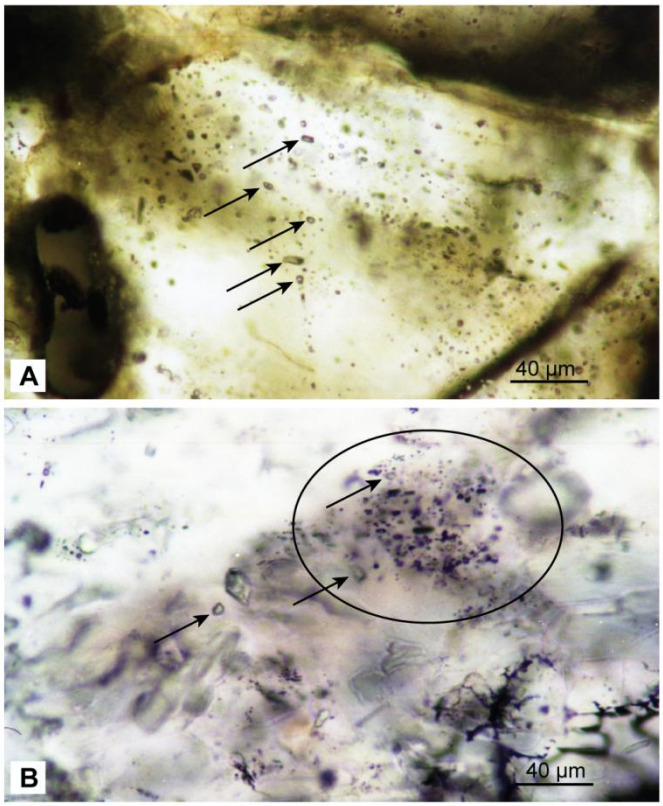

Figure 7

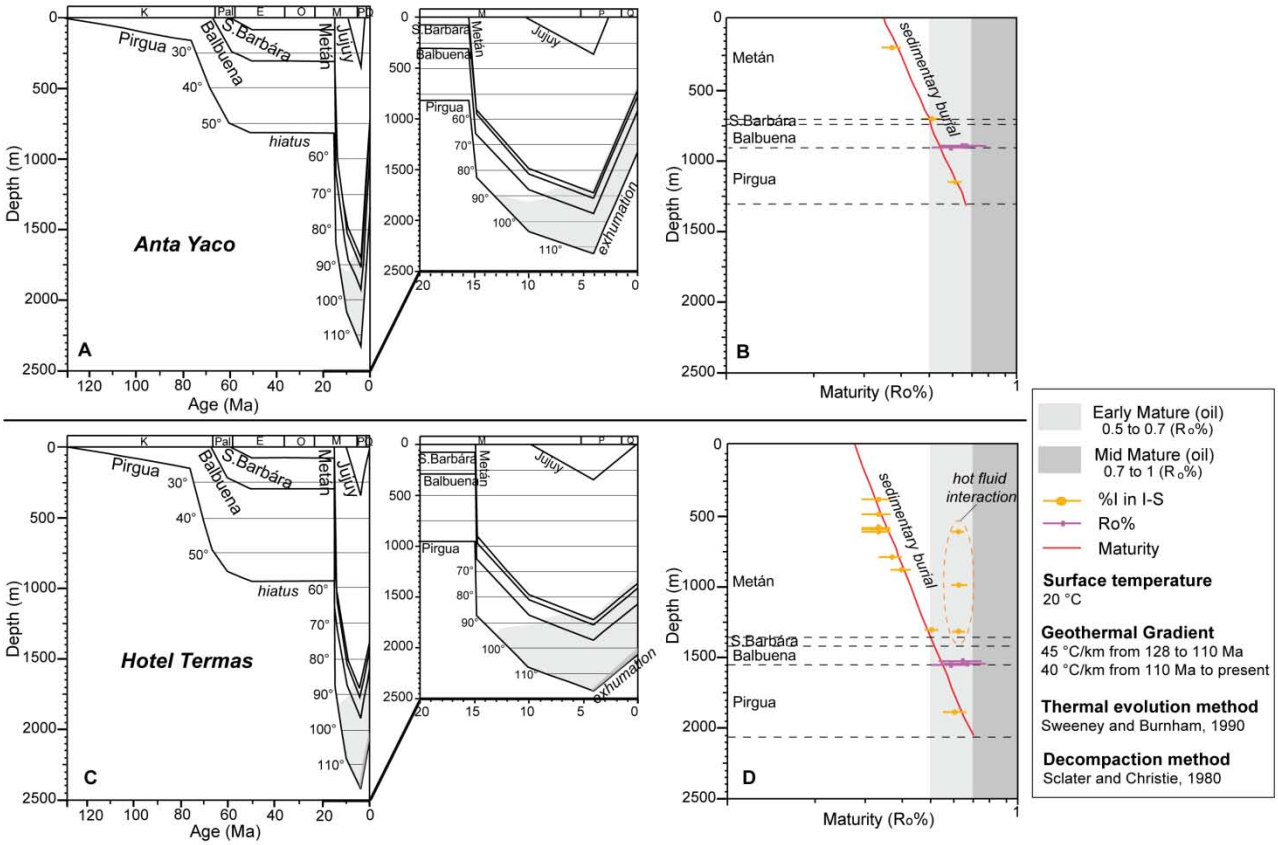

Figure 8

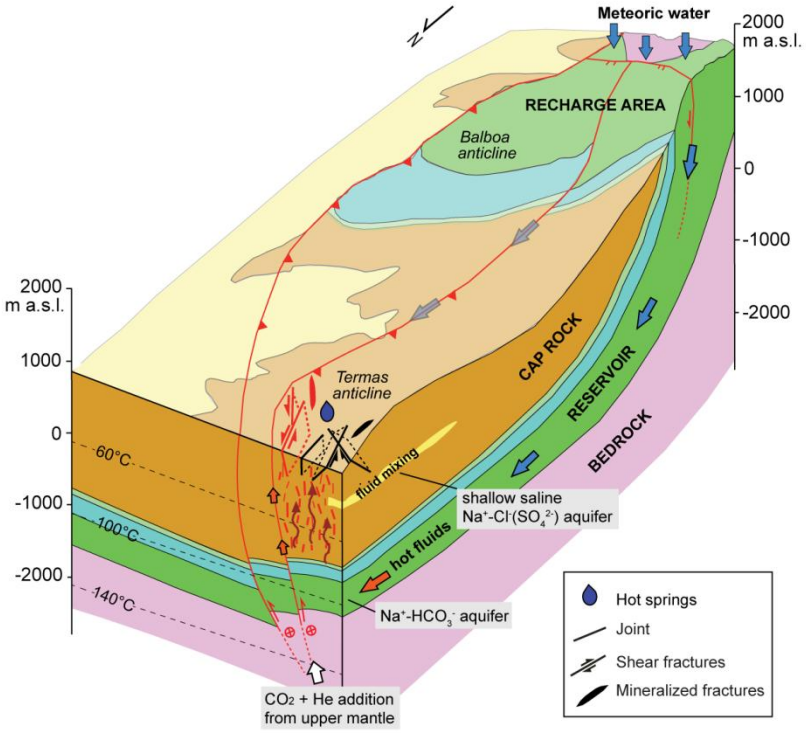

Figure 9

Highlights

1. We investigate the thermal state of the geothermal cap rock
2. We compare features and distribution of fractures with paleothermal indicators
3. We highlight a localized thermal alteration of the cap rock due to fluid migration
4. We define the main pathways of hot fluids
5. We demonstrate that cap rock regionally act as good thermal insulator